

Anisotropic Friedel oscillations in graphene-like materials: The Dirac point approximation in wave-number dependent quantities revisited

Tohid Farajollahpour^{1,2}, Shirin Khamouei^{1,+}, Shabnam Safari Shateri^{3,+}, and Arash Phirouznia^{1,2,*}

¹Department of Physics, Azarbaijan Shahid Madani University, 53714-161, Tabriz, Iran

²Condensed Matter Computational Research Lab. Azarbaijan Shahid Madani University, 53714-161, Tabriz, Iran

³Department of Physics, University of Bonab, Bonab, East Azarbaijan, Iran

*phirouznia@azaruniv.ac.ir

ABSTRACT

Friedel oscillations of the graphene-like materials are investigated theoretically for low and intermediate Fermi energies. Numerical calculations have been performed within the random phase approximation. For intra-valley transitions it was demonstrated that the contribution of the different Dirac points in the wave-number dependent quantities, such as dielectric function $\epsilon(\vec{q})$, has been determined by the orientation of the wave-number with respect to the Dirac point position vector in k -space. Therefore identical contribution of the different Dirac points is not automatically guaranteed by the degeneracy of the Hamiltonian at these points. Meanwhile it was shown that the contribution of the inter-valley transitions is always anisotropic even when the Dirac points coincide with the Fermi level ($E_F = 0$). This means that the Dirac point approximation based studies give the correct physics only at high wave length limit. The anisotropy of the static dielectric function reveals different contribution of the each Dirac point. Additionally, the anisotropic k -space dielectric function results in anisotropic Friedel oscillations in graphene-like materials. Increasing the Rashba interaction strength slightly modifies the Friedel oscillations in graphene-like materials. Therefore the anisotropic dielectric function in k -space is the clear manifestation of band anisotropy in the graphene-like systems.

At the present time two dimensional structures are one of the most rich and fast growing fields of condensed matter physics. Experimental observation of graphene in 2004^{1,2} has created a great motivation in scientists to the discovery and study of the other possible two-dimensional (2D) allotropes of IV group elements in periodic table such as silicene, germanene³ and recently stanene.^{4,5} These new 2D materials and other buckled honeycomb lattice structures predicted in theoretical works⁶⁻⁹ and several experimental synthesization have also been performed for realization of these materials.¹⁰⁻¹³ The silicon and germanium analog of graphene with slightly buckled honeycomb geometry were predicted to have a Dirac cone and the electrons follow the massless Dirac equation near the Fermi level.⁶⁻⁸ Unlike graphene, the hybridization of π bonds in silicene is not pure and the structure of silicene shows a mixed hybridization. The π electrons in silicene are much more active than graphene and this lead to a different structure from graphene.¹⁴ Similar to the graphene structure, silicon atoms are arrayed in a hexagonal lattice, but with a slight buckling that proved by first principle studies which show low buckled silicene is thermally stable (Fig. 1).⁷ It was also shown that the electronic dispersion of the silicene near K points of the first Brillouin zone is linear similar to the behavior of Dirac materials.^{6,7,15,16} Since the flat configuration of silicene is not stable⁷ the buckled configuration of silicene is more interesting for research activities. The spin orbit coupling (SOC) in silicene is more stronger than graphene which leads to relatively large energy gap at the Dirac points. Strong SOC in silicene makes this monolayer a good candidate for topological insulators and quantum spin Hall effect (QSHE).^{8,17-19}

It has been generally assumed that the degeneracy of the Dirac points provides the identical contribution of these points in the physical quantities. This could be a correct procedure and would be valid for calculation of the scalar quantities. However, it should be noted that the Dirac points in k -space are not distributed isotropically. This anisotropy has been dictated by the band anisotropy of the honeycomb structures in the k -space. Therefore identical treatment of the Dirac points automatically ignores anisotropy of the band energy. It seems that this anisotropy could be appeared just at high Fermi energies. However, as it was shown in this work, even in the case of low Fermi energies where the Fermi level could match the Dirac points the contribution of inter-valley transitions are completely anisotropic.

Within the Dirac point approximation when the Dirac points have been treated identically, anisotropic effects have been completely ignored at low Fermi energies. Some of the anisotropic effects are raised by increasing the Fermi energy up to the

Table 1. Lattice constant and Energy scales for graphene and other buckled honeycomb materials.^{8, 25–27}

material	a	t	t_{SO}	t_{intR}
silicene	3.86 Å	1.6 eV	0.75 meV	0.46 meV
germanene	4.02 Å	1.3 eV	8.27 meV	7.13 meV
graphene	2.46 Å	2.8 eV	0.00114 meV	—

range of trigonal warping effects. However, even at low Fermi energies, band anisotropy of the system manifests itself in the dielectric function $\varepsilon(\vec{q})$, at least at the range of inter-valley transitions where $q \sim |\mathbf{K}_D - \mathbf{K}'_D|$ in which \mathbf{K}_D and \mathbf{K}'_D are different Dirac points. At the level of low Fermi energies, the band energy of the system has been reduced to a cone-like dispersion. In this case the Fermi level has been identified with a symmetric circle around the Dirac points known as Fermi circle. Calculation of the wave number dependent quantities should be performed with some care, since the direction of the transferred momentum \vec{q} , determines the contribution of each Dirac point in both intra-valley and inter-valley transitions. For a given transferred momentum \vec{q} , different Dirac points have not the same contribution in this type of the physical quantities. This could be considered as another type of anisotropic behaviors in wave number dependent quantities that originate from non-identical contribution of the Dirac points. This work attempts to provide some insight into the limitations of identical treatment of the Dirac points. Results of the current work emphasize the need for a systematic revision of identical treatment of the Dirac points in different types of quantities. Specifically, we analyze the robustness of the band anisotropy in graphene and other honeycomb systems which manifests itself in the dielectric function and Friedel oscillations of the system. To this end, random phase approximation (RPA)²⁰ is employed beyond the Dirac point approximation. In this case at low Fermi energies, validity of the identical contribution of the Dirac points in the dielectric function could be examined within this approach.

It is obvious that the contribution of the nonlinear part of the energy dispersion at high Fermi energies could be given beyond the Dirac point approximation. If we use the same approach at the level of low Fermi energies. This ensures us that the correct contribution of each Dirac point has been taken into account. It can be shown that even at low Fermi energies the band induced anisotropy could be observed in graphene-like materials. Meanwhile the anisotropic effects which have been observed at low Fermi energies have nothing to do with the nonlinear part of the energy dispersion which is available beyond the Dirac point approximation. This could be understood if we consider that band anisotropy is present both at high and low energy limits. The unique optical and electronic properties of graphene-like systems such as silicene has made these materials a good candidate for plasmonics applications. Meanwhile plasmonic-based studies has already been performed for graphene however, the other graphene-like systems are known as highly appealing subjects for this field of condensed matter physics.^{21–24}

Friedel oscillation has been reported for graphene in low energy Hamiltonian which relies on the Dirac-cone approximation.^{28–31} It is important to note that the information about the possible topological phase transitions could be captured by Friedel oscillations. Results of the Friedel oscillations in silicene demonstrates that there is a connection between the Friedel oscillations and topological phase transition.³² These approaches ignore the contribution comes from the nonlinear part of the spectrum and can be reasonable when the Fermi energy is close to the Dirac points. Nevertheless, as mentioned before identical treatment of the Dirac points within the Dirac point approximation cannot capture the anisotropic contribution of these points in wave-number dependent quantities. In this work calculations have been performed beyond the Dirac point approximation in which all possible types of the band anisotropy, including the nonlinear and linear parts of the spectrum, could be considered. Meanwhile, it should be noted that the linear dispersion at Dirac points and even existence of Dirac cones in silicene is being seriously debated.^{33,34} Motivated by the mentioned points, we have performed current numerical study to obtain a better understanding about the limitations of the Dirac point approximation in graphene-like systems.

Theoretical framework

Graphene-like materials could be considered as honeycomb lattice structures, similar to graphene meanwhile the SOC of buckled honeycomb structures contains parallel and perpendicular terms. The Hamiltonian of the buckled honeycomb lattice in tight-binding approximation in the presence of SOCs can be written as

$$H = -t \sum_{\langle ij \rangle \alpha} c_{i\alpha}^\dagger c_{j\alpha} + it_{SO} \sum_{\langle\langle ij \rangle\rangle \alpha\beta} u_{ij} c_{i\alpha}^\dagger \sigma_{\alpha\beta}^z c_{j\beta} - it_{intR} \sum_{\langle\langle ij \rangle\rangle \alpha\beta} \mu_{ij} \hat{c}_{i\alpha}^\dagger \left(\vec{\sigma} \times \vec{d}_{ij} \right)_{\alpha\beta}^z \hat{c}_{j\beta} + it_{extR} \sum_{\langle ij \rangle \alpha\beta} \hat{c}_{i\alpha}^\dagger \left(\vec{\sigma} \times \vec{d}_{ij} \right)_{\alpha\beta}^z \hat{c}_{j\beta} \quad (1)$$

where the operator $c_{j\alpha}^\dagger$ ($c_{j\alpha}$) creates (annihilates) an electron with spin α at site j and t is the nearest neighbor hopping amplitude. The values of these parameters for different materials are given in table 1. The t_{SO} is the next-nearest neighbor

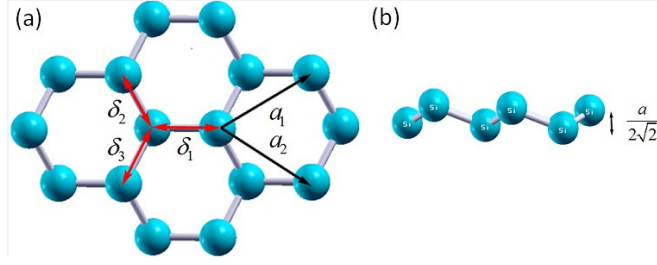


Figure 1. (a) Hexagonal structure of buckled two dimensional lattice where $\delta_1 = a \left(1, 0, 1/2\sqrt{2} \right)$, $\delta_2 = \frac{a}{2} \left(-1, \sqrt{3}, 1/\sqrt{2} \right)$, $\delta_3 = \frac{a}{2} \left(-1, -\sqrt{3}, 1/\sqrt{2} \right)$ are the nearest neighbors position vectors, the lattice vectors are $a_1 = \frac{a}{2} (3, \sqrt{3})$, $a_2 = \frac{a}{2} (3, -\sqrt{3})$, and the next nearest position vectors are $\delta'_1 = \pm a_1$, $\delta'_2 = \pm a_2$ and $\delta'_3 = \pm(a_2 - a_1)$. (b) Side view of buckled structure for silicene.

hopping, $u_{ij} = \vec{d}_i \times \vec{d}_j / |\vec{d}_i \times \vec{d}_j|$ where \vec{d}_i and \vec{d}_j are the two nearest bonds that connect the next-nearest neighbors, Where $u_{ij} = 1$ if the next-nearest neighbor hopping is counterclockwise and $u_{ij} = -1$ when it is clockwise with respect to the positive z axis.³⁵ The $\langle\langle ij \rangle\rangle$ run over all the next-nearest neighbor hopping sites and σ_z is the Pauli matrix. t_{intR} and t_{extR} are the strength of intrinsic and extrinsic Rashba SOC's respectively and $\mu_{ij} = +1(-1)$ stands for the A (B) site. The strength of the external Rashba coupling can be manipulated by an external gate voltage or by the selected substrate. The extrinsic Rashba coupling arises as a result of the inversion symmetry breaking due to an applied perpendicular electric field or interaction with substrate.³⁶

Dielectric function and the screening of the charged impurity and also the dynamical polarization which gives collective excitations could be captured by the polarization function $\Pi(\omega, q)$. Dielectric function and collective density oscillations of an electron liquid (plasmons), have been observed in different metals and superconductors.^{37,38} At the static limit ($\hbar\omega = 0$) polarization function gives the screening behavior of the coulomb potential. The dielectric function is relevant to plasmonic studies meanwhile the transport and phonon spectra are also another relevant fields.³⁹ The electron-electron interaction has been

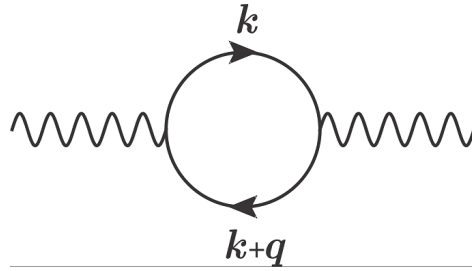


Figure 2. The bare polarization bubble diagram corresponding to Eq. (3).

considered within the random phase approximation characterizes by the density-density correlation function or polarization function (Fig. 2).^{20,28,29,38,40-45} In this approach dielectric function is given by

$$\varepsilon(\omega, \vec{q}) = 1 - V(q) \Pi(\omega, \vec{q}) \quad (2)$$

Where $V(q)$ is the 2D Coulomb potential, here $V(q) = 2\pi e^2/q$. Within the Dirac point approximation an effective Coulomb potential could be employed in which $V(q) = 2\pi\alpha/q$ and α is the ratio of coulomb to kinetic energy and named effective fine structure constant where equal to $\alpha = e^2/(\hbar\varepsilon_0 v)$ and ε_0 is the bare dielectric constant. Unlike to the graphene where the value of fine structure constant could be determined experimentally in different substrates,⁴⁶ for other buckled honeycomb lattices one can set $\alpha = 0.8$.²³ The polarization function in one loop approximation is calculated directly from the bubble diagram that shown in Fig (2).

$$\begin{aligned} \Pi(\omega, \vec{q}) &= \sum_{ss'kk'} \frac{f_k^s - f_{k'}^{s'}}{\omega + E_k^s - E_{k'}^{s'}} | \langle k' \lambda_{k'}^{s'} | e^{iq \cdot r} | k \lambda_k^s \rangle |^2 \\ &= \sum_{ss'k} \frac{f_k^s - f_{k+q}^{s'}}{\omega + E_k^s - E_{k+q}^{s'}} F_{s's}(\vec{k} + \vec{q}, \vec{k}), \end{aligned} \quad (3)$$

here, the summation performed over the full Brillouin zone and all of the spin and pseudo-spin dependent eigenstates in which $f_k^s = \frac{1}{\exp\beta(E_k^s - E_F) + 1}$ is the Fermi distribution function, and E_F is the Fermi energy. The form factor is given by $F_{s',s}(\vec{k}', \vec{k}) = |\langle k' \lambda_{k'}^{s'} | e^{iq \cdot r} | k \lambda_k^s \rangle|^2 = |\langle k' \lambda_{k'}^{s'} | k \lambda_k^s \rangle|^2 \delta_{\vec{k}', \vec{k} + \vec{q}}$ in which $|k \lambda_k^s \rangle = |k \rangle \otimes |\lambda_k^s \rangle$ are the eigenstates of the Hamiltonian where $|\lambda_k^s \rangle$ is the eigenstate in the spin and pseudo-spin subspaces. $\delta_{\vec{k}', \vec{k} + \vec{q}}$ represents the momentum conservation rule as a general condition for contributing transitions.

Within the Dirac point approximation the above expression of the polarization function has been assumed to be²⁹

$$\Pi(\omega, \vec{q}) = g \sum_{ss'k} \frac{f_k^s - f_{k+q}^{s'}}{\omega + E_k^s - E_{k+q}^{s'}} F_{s's}(\vec{k} + \vec{q}, \vec{k}) \quad (4)$$

where g is valley degeneracy factor and the summation runs around a single Dirac point. Moreover in the absence of the spin-orbit interactions the form factor is reduced to: $F_{s's}(\vec{k} + \vec{q}, \vec{k}) = \frac{1}{2}[1 + ss' \cos(2\theta)]$, with θ being the angle between k and $k + q$. It should be noted that in this relation the degeneracy factor, g , implies identical contribution of the different Dirac points in the polarization function at given \vec{q} . As discussed before the valley degeneracy could result in identical contribution of the Dirac points in scalar quantities such as total energy. Nevertheless this degeneracy cannot indicate the identical contribution of the Dirac points in the wave number dependent quantities such as polarization function. Consequently, this type of calculations should be performed beyond the Dirac point approximation even when the Fermi energy level lies close to the cones intersecting points. This is due to the fact that the contribution of the different Dirac points, \vec{K}_D and \vec{K}'_D , is not the same and depends on the location of the Dirac point in the k -space that has been identified by \vec{K}_D .

When the integration has been reduced to the Fermi circle of a single Dirac point this assumption automatically ignores the contribution of the inter-valley transitions in which the initial and final states belong to different Fermi circles. This could take place when the transferred momentum, q , satisfies $q \sim |\vec{K}_D - \vec{K}'_D|$. This means that the general form of the Dirac point approximation ignores the inter-valley transition. The anisotropy of the dielectric function results from this type of transitions when the Fermi energy is exactly zero.

Within a second-order perturbation approach it has been realized that the exchange interaction of the localized spins S_1 and S_2 with the conducting electrons results in an effective magnetic interaction between these localized magnetic moments known as RKKY interaction given by⁴⁷ $H_{RKKY}(r) = JS_1 \cdot S_2 \Pi(r)$ in which J is the exchange coupling constant between the conducting electrons and localized magnetic moments and $\Pi(r)$ is the Fourier transform of the k -space polarization function $\Pi(q)$. Therefore the characteristic properties of this interaction could be captured by the polarization function of the mediating electrons. Accordingly it is expected that the anisotropy of the polarization function could manifest itself in the anisotropy of the RKKY interaction as it appeared in the dielectric function.

The polarization function could be separated into the inter-band (if $s \neq s'$) and the intra-band (if $s = s'$) contributions.⁴⁴ In addition each of these contributions could be classified as intra-valley and inter-valley contributions that correspond to different transitions in which the transferred momentum, \vec{q} , is $q \leq k_F < |\mathbf{K}_D - \mathbf{K}'_D|$ or $q \sim |\mathbf{K}_D - \mathbf{K}'_D|$ respectively (where k_F is the radius of the Fermi circle and $\mathbf{K}_D, \mathbf{K}'_D$ are different Dirac points). To illustrate the oscillations of the induced charge density a charged impurity has been considered to be inserted in the honeycomb structure. The static polarization function is of particular importance as it determines the screened potential of a charge impurity. The screening particle density $\delta n(r)$ due to the central impurity Ze is,

$$\delta n(\vec{r}) = Ze \frac{1}{(2\pi)^2} \int \left[\frac{V(\vec{q}) \Pi(0, \vec{q})}{\epsilon(0, \vec{q})} \right] \exp(i\vec{q} \cdot \vec{r}) d^2 q. \quad (5)$$

It is really important to note that the above integration goes beyond the limit of intra-valley transitions (the radius of Fermi circle) and therefore the contribution of the inter-valley transitions should be included. This means that the pattern of Friedel oscillations requires the whole information of the static response function in the first Brillouin zone. Therefore inter-valley transitions between the different Dirac cones should be included. Therefore this type of transitions cannot be captured within the single Dirac cone approximation.

We want to remark that the Friedel oscillation curves in the RPA, Hubbard vertex correction and Singwer-Sjölander are very similar.^{20,48,49} The reason, for example in the Hubbard Model, is that the Hubbard local field factor $G_H(q)$ is appeared in correlations that are deal with two-body or more, however the screening is essentially a one-body property and the correlations are not appear in one-body amplitudes.²⁰

Non-identical contribution of different Dirac cones

As depicted in Fig. (3) at low Fermi energies the Fermi curves have been appeared as separated islands around each Dirac point. Therefore the amount of the dielectric and polarization functions in a given \vec{q} wave number have significantly been

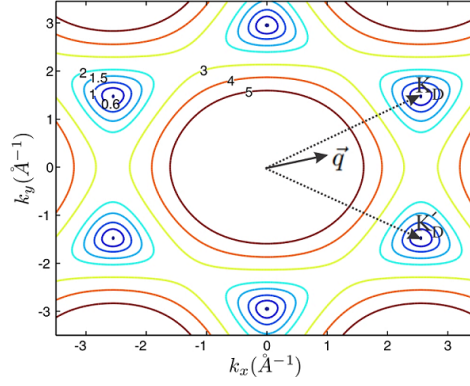


Figure 3. Dirac points of monolayer graphene and Fermi curves at different Fermi energies. Fermi contours have been depicted for $E_F = 0.6eV, 1.0eV, 1.5eV, 2.0eV, 3.0eV, 4.0eV$ and $5.0eV$. For a given wave vector \vec{q} the contribution of the different Dirac points on $\varepsilon(\vec{q})$ strictly depends on the orientation and position of the \vec{q} with respect to the six Dirac vectors. Trigonal warping of the Fermi curves at different Fermi energies has also indicated in this figure. Single Dirac cone approximation could take into account the anisotropic effects comes from the trigonal warping of a single Fermi curve, however, since the orientation of the deformed Fermi curves are not the same, the anisotropic contribution of the other cones are not identical.

determined by the orientation of the wave number with respect to the Dirac points position vectors. This anisotropy of the q -space is reflected in the real space quantities such as Friedel oscillations.

When the Fermi level is appeared as distinct circular curves in k -space. One might conclude that the circular shape of the Fermi contour around of the Dirac points implies that all of the extractable physical properties of the system should be isotropic as long as the Dirac point approximation is applied. However it should be considered that the isotropic and circular shape of the Fermi contours around each of the Dirac points cannot results in isotropic properties at least in when the inter-valley transitions are taken into account. This is due to the anisotropy of the band structure in honeycomb systems which indicates that the Dirac points themselves are located in k -space in an anisotropic manner. Accordingly it is important to note that the results of present study cannot be compared with the results that have been obtained within the single Dirac point approximation.⁵⁰

Meanwhile, for calculation of vector and tensor dependent quantities we should consider that the contribution of inter-valley transitions cannot be identical in all of the q -space directions even when $E_F = 0$. Moreover when $E_F > 0$ both of the intra-valley and inter-valley transitions result in anisotropic dependence of the dielectric function in q -space. Therefore different directions in of a given momentum transfer, q , have not identical contribution even when the Dirac points are degenerate. Accordingly the conventional Dirac point approximation could not describe all of the physics of the vector or vector dependent parameters at low wave-length limit. This could also result in anisotropic electric and thermal conductivity in graphene-like materials for short range scatterers (for example in the case of the delta-shaped scatterers) in which all of the intra-valley and inter-valley scatterings are possible.

When the Dirac points are not located exactly on the Fermi level the intra-valley transitions could take place within the range of $q \leq k_F$. Meanwhile we have assumed that the Fermi energy is still low enough to employ the linear dispersion relation of the Dirac cone. It can be shown that both of the intra-valley ($q \leq k_F$ for this case) and inter-valley transitions should be considered as anisotropic contributions in the dielectric function. In this case since the inter-band transitions ($|k\lambda_k^s \rangle \rightarrow |k'\lambda_{k'}^{s'} \rangle$, $s \neq s'$) are absent in the static limit ($\hbar\omega = 0$) therefore all of the contributing terms (both intra-valley and inter-valley transitions) are intra-band. Consequently, the contribution of $q \sim 0$ transitions in the static dielectric function decreases by increasing the Fermi energy. Since it can be shown that for $E_F \neq 0$ we have $F_{ss'}(\vec{k} + \vec{q}, \vec{k}) = 0$ when $q = 0$ and $s \neq s'$.

Different types of transitions could be contributed in the dielectric function of the honeycomb structures. In this case transitions could be either intra-valley or inter-valley. Where in the intra-valley transitions initial and final states \vec{k} and \vec{k}' belong to the same Dirac valley cone while in the inter-valley transitions \vec{k} and \vec{k}' belong to different Dirac cones (Fig. 4 (a) and (b)). The momentum conservation rule for each transition between the states \vec{k} and \vec{k}' with transferred momentum \vec{q} could be satisfied when \vec{k} and \vec{k}' sweep the Fermi circles as shown in Fig. 4. It can be inferred that this condition could be satisfied for intra-valley transitions when $0 \leq q \leq k_F$ where k_F is the radius of the Fermi circle Fig. 4 (a) and inter-valley transitions could take place $q \sim |\mathbf{K}_D - \mathbf{K}'_D|$ where \mathbf{K}_D and \mathbf{K}'_D are different Dirac points.

Fig. 4 shows the Fermi circles of a planar honeycomb lattice has been depicted in the absence of the SOCs. It can be shown that due to this six-fold band rotational symmetry of the system if the transition rule is satisfied for a given transferred

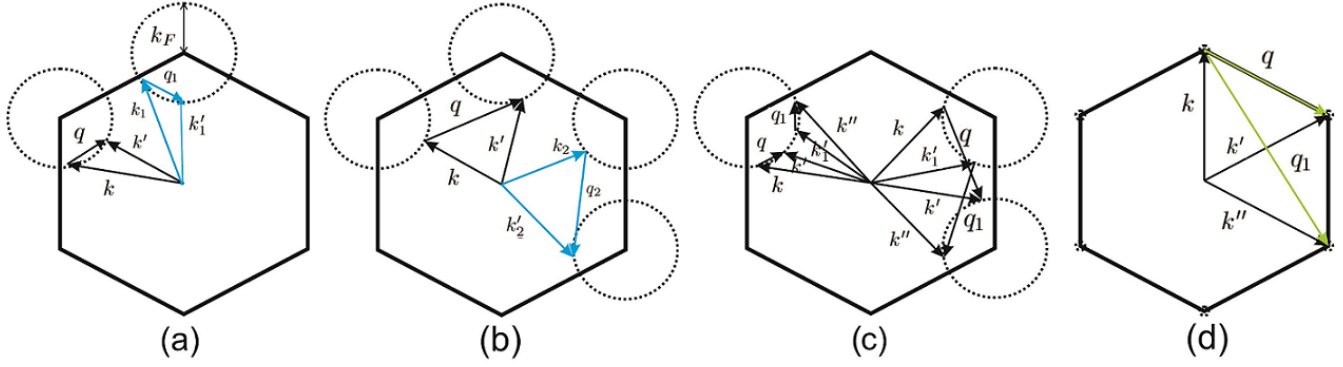


Figure 4. (Color online) Intra-valley (a) and inter-valley (b) transitions for a given transferred momentum \vec{q} . Dashed circles indicate the Fermi circles of the honeycomb system in the absence of the spin-orbit couplings. When the momentum conservation rule is satisfied for \vec{q} the initial and final states should be placed on the Fermi circles. In this case the contribution of the given states (black vectors) is identical with the contribution of the sixfold-rotated states (cyan vectors). One can imagine about another type of possible transitions (c) with constant value of the transferred momentum $q = q_1$ between the equi-energy states $E_k^s = E_{k'}^s = E_{k_1}^s = E_{k''}^s$, where the corresponding pair vectors (\vec{q}, \vec{q}_1) , (\vec{k}, \vec{k}_1) and (\vec{k}', \vec{k}'') are not related by sixfold symmetry operators e.g. $\mathcal{R}_{2\pi/6}^n \vec{q} \neq \vec{q}_1$. It can be shown that form factor of these transitions are different i.e. $F(k, k') \neq F(k_1, k'')$. At zero Fermi energy (d) i.e. when $k_F = 0$ intra-valley transitions occur at $q = 0$ which result in central peak of the dielectric function. However inter-valley transitions (light green vectors) are still the source of anisotropy of the dielectric function.

momentum (\vec{q}) it will also be satisfied for the sixfold rotated wave number $\mathcal{R}_{2\pi/6}^n \vec{q}$ (Fig. 4 (a) and (b)). In which $\mathcal{R}_{2\pi/6}$ is the sixfold rotation operator. This means that

$$\begin{aligned} \delta_{\vec{k}+\vec{q}, \vec{k}'} &= \delta_{\mathcal{R}_{2\pi/6}^n \vec{k} + \mathcal{R}_{2\pi/6}^n \vec{q}, \mathcal{R}_{2\pi/6}^n \vec{k}'} \\ &= \delta_{\vec{k}_n + \vec{q}_n, \vec{k}'_n} \end{aligned} \quad (6)$$

Meanwhile the form factor of the graphene is also invariant under the sixfold rotations in the absence of the spin-orbit couplings.

$$F_{s's}(\vec{k} + \vec{q}, \vec{k}) = F_{s's}(\mathcal{R}_{2\pi/6}^n \vec{k} + \mathcal{R}_{2\pi/6}^n \vec{q}, \mathcal{R}_{2\pi/6}^n \vec{k}). \quad (7)$$

In both cases i.e. for inter-valley and intra-valley transitions band symmetry of the honeycomb structures manifests itself as $E_{\vec{k}}^s = E_{\mathcal{R}_{2\pi/6}^n \vec{k}}^s$. Therefore Eq. 3 reveals that for a given transferred momentum, \vec{q} , satisfying the transition rule $\vec{k} = \vec{k}' - \vec{q}$. The contribution of the \vec{k} -state in the dielectric function is identical with the contributions of the rotated states: $\mathcal{R}_{2\pi/6} \vec{k}, \mathcal{R}_{2\pi/6}^2 \vec{k}, \dots, \mathcal{R}_{2\pi/6}^5 \vec{k}$ regardless of the inter-valley or intra-valley nature of the transitions. In the other words it could be inferred that $\varepsilon(\vec{q}) = \varepsilon(\mathcal{R}_{2\pi/6} \vec{q}) = \varepsilon(\mathcal{R}_{2\pi/6}^2 \vec{q}) \dots = \varepsilon(\mathcal{R}_{2\pi/6}^5 \vec{q})$. For example in the case of intra-valley transitions the different Dirac point or Fermi curves which have been related by sixfold rotation operators have the same contribution in the dielectric function for those transferred momentums which have the same symmetry relation. Consequently, the contribution of the Fermi circle located around the \vec{K}_D Dirac point on the dielectric function of \vec{q} is identical with the contribution of $\vec{K}_D^{(i)}$ Fermi circle on the dielectric function of $\mathcal{R}_{2\pi/6}^i \vec{q}$ where these two Dirac points are related by $\vec{K}_D^{(i)} = \mathcal{R}_{2\pi/6}^i \vec{K}_D$. If we continue the same procedure for parallel wave numbers, which satisfying the transition rule, one can realize the anisotropy of the dielectric function which manifests itself by sixfold symmetric curve at low transferred momentums Fig. ???. These relations identify different class of the states which have identical contribution in the dielectric function i.e. the for different states with transferred momentum q in this case the class of the identical contributions for both inter and intra valley transitions is specified by

$$[q] = \{\vec{q}, \mathcal{R}_{2\pi/6} \vec{q}, \mathcal{R}_{2\pi/6}^2 \vec{q}, \dots, \mathcal{R}_{2\pi/6}^5 \vec{q}\}. \quad (8)$$

Which corresponds to the transitions: $\vec{k} \rightarrow \vec{k} + \vec{q}, \mathcal{R}_{2\pi/6}^5 \vec{k} \rightarrow \mathcal{R}_{2\pi/6} \vec{k} + \mathcal{R}_{2\pi/6} \vec{q}, \dots, \mathcal{R}_{2\pi/6}^5 \vec{k} \rightarrow \mathcal{R}_{2\pi/6} \vec{k} + \mathcal{R}_{2\pi/6} \vec{q}$.

The first consequence of the above argument is that the different Fermi curves of each Dirac point have not identical contribution on the dielectric function at a given \vec{q} wave number. In the other words the contribution of each Fermi circle (corresponding to K_D dirac point) with a given transferred momentum, \vec{q} , has been determined by the orientation of the \vec{q} with

respect to the K_D . When \vec{q} satisfies the transition rule for a specific Dirac cone (for example in an intra-valley process) this rule will be satisfied for $\mathcal{R}_{2\pi/6}^n \vec{q}$ ($n = 1..5$) at other Dirac cones and \vec{q} itself could not satisfy the momentum conservation rule or could not give the same contribution at these Dirac cones. Therefore the contribution of different Fermi circles on the dielectric function of \vec{q} is not identical. Accordingly the dielectric function should be anisotropic in the q -space with sixfold symmetry which was originated from the symmetry of the band structure.

All of the other possible transitions with a given fixed value of the transferred momentum could take place between the isoenergy states as shown in Fig. 4 (c). In this group of the transitions, transferred momentum is the same $q = q_1$ and both of the initial final states are located at Fermi circle $E_k^s = E_{k'}^s = E_{k_1'}^s = E_{k''}^s = E_F$. However, corresponding pair vectors are not related by sixfold symmetry operators i.e. $\mathcal{R}_{2\pi/6}^n \vec{q} \neq \vec{q}_1$, $\mathcal{R}_{2\pi/6}^n \vec{k} \neq \vec{k}_1'$ and $\mathcal{R}_{2\pi/6}^n \vec{k}' \neq \vec{k}''$. The transition rule has been satisfied for these transition where we have $\vec{k} + \vec{q} = \vec{k}'$ and $\vec{k}_1' + \vec{q}_1 = \vec{k}''$. Meanwhile, the form factor of the transitions are not the same $F(k, k') \neq F(k_1', k'')$ which implies that the corresponding contributions are not identical (Fig. 4 (c)).

When the Fermi energy located at Dirac points i.e. $E_F = 0$ then the intra-valley transitions occur in $\vec{q} = 0$ between different bands (Fig 4 (d)). Unlike the previous case the intra-valley contributions are identical here. These contributions result in the central peak of the dielectric function. Since the $V(q) = 2\pi e^2/q$ diverges at $q = 0$ where the intra-valley transitions could contribute at this point. However the inter-valley transitions occur away from the Γ -point ($q = 0$) result in anisotropic contributions as the previous case. Therefore one can expect that the anisotropy of the dielectric function would be appeared at $q \geq |\mathbf{K}_D - \mathbf{K}'_D|$ Fig. (7).

Discussions and numerical results

In conclusion, we have analyzed the band induced anisotropic effects in graphene-like structures. We have also investigated the influence of the spin-orbit interactions on dielectric function and Friedel oscillations in this type of materials.

Due to the foregoing discussions for wave number-dependent or non-scalar quantities such as dielectric function, electric and thermal conductivities we have to concern about the position of the Dirac points relative to the direction of the characteristic vector of the physical quantity (such as transferred momentum) even when the Dirac point approximation is valid. For sharp scattering potentials we have to consider the inter-valley transitions in this type of the quantities. Within the Dirac point approximation the integration over the state-resolved contributions is generally performed over a single Fermi circle. This could be a correct approach when we assume the identical contribution of each Dirac point and ignore the inter-valley transitions. In this case if we put aside the Dirac point approximation and perform the integration over the whole Brillouin zone the correct contribution of each Dirac point could be obtained. This means that beyond the Dirac point approximation dielectric function and therefore Friedel oscillations for graphene-like honeycomb structures should be anisotropic in k -space and the real space respectively.

Based on RPA formalism, which accounts for electron-electron scattering, we have shown that the Dirac points have not identical contribution for wave number dependent quantities such as dielectric function even when the Fermi energy is close to these points.

The main limitations for the use of the Dirac point approximation has been discussed within the current work. Non-identical contribution of the Dirac points results in anisotropic dielectric function in k -space. Moreover, the anisotropy of the dielectric function leads to anisotropic Friedel oscillation in graphene-like materials. We have shown that the isotropic Friedel oscillations cannot be considered as a consequence of the Dirac point approximation itself. Since in this case the isotropic Friedel oscillations could be obtained just when the inter-valley transitions are ignored.

The influence of the Rashba SOC on the dielectric function and Friedel oscillations has also been discussed in the present study where we have shown that increasing the Rashba coupling strength cannot results in significant change in the dielectric function and Friedel oscillation. Meanwhile in the presence of the Rashba interaction the inversion symmetry of the dielectric function has been lifted in k -space. The extrinsic Rashba interaction could be manipulated by an external gate voltage. By changing the extrinsic Rashba coupling strength, polarization function and consequently the dielectric function will be altered. Dielectric function has been determined by density-density correlations in the system. In the present work this correlation function has been obtained within the random phase approximation. Results of the numerical calculations depicted in the following figures of this section.

As mentioned before the band induced anisotropic effects could be obtained even when the Fermi energy is close to the Dirac points. This is due to the fact that the optical transitions which could be available for a given transferred momentum \vec{q} are not identical for different Dirac points in k -space. At the level of the single Dirac point approximation anisotropic position of the Dirac points and its relevant effects have been ignored. Meanwhile, the anisotropy of single Fermi circle reshaping, which arises by increasing the Fermi energy, could be obtained within the single Dirac cone approximation. In the present work we have obtained the anisotropic properties which could be originated from the anisotropic location of the Dirac points at low Fermi energies.

According to the numerical results, two-dimensional graphene like materials show anisotropic Friedel oscillations beyond the Dirac cone approximation even when the Dirac points located at the Fermi level. In addition results of the present study show that the extrinsic Rashba coupling has not any considerable effect on the Friedel oscillations. Meanwhile the influence of the spin-orbit couplings is relatively evident in the Friedel oscillations of the monolayer germanene.

It is important to consider that the general integral expression for the polarization function (Eq. 3) goes beyond the states in which the Dirac point approximation is not valid. Nevertheless, far from the Dirac points most of the states in each band are empty with no contribution in the dielectric function in the static limit ($\hbar\omega = 0$) even at room temperature. For gap-less structures, at room temperature, thermal transitions could be taken place within the range of thermal energy $K_B T = 0.025 \text{ eV}$. Therefore, when the Fermi level is located at the Dirac point, the contribution of the states which were not in the permitted range of the Dirac point approximation automatically have been eliminated by the distribution function implemented in Eq. (3).

The linear dispersion relation (and therefore circle like Fermi curves) around the Dirac points valid even up to $E_F \sim 1 \text{ eV}$ in graphene and the thermal transitions at room temperature with $K_B T = 0.025 \text{ eV}$ could not induce any considerable contribution from those states which have been located far from the Dirac points. So it seems that the Dirac point approximation could still describe the physics of the honeycomb lattice and the linear dispersion relation around the Dirac points could be employed for the calculation of the dielectric function. This means that the non-linear part of the band structure and the anisotropy that might be induced by this part could be ignored. This is due to the fact that this part of the band structure (which could be considered the energy states with $E_k^s > 1 \text{ eV}$) has not been occupied even as a result of the thermal transitions or could not contribute in the isoenergy transitions of the static limit. However, in the current work we have shown that the contribution of the Dirac points in wave-number dependent quantities should be calculated with some care even when the Dirac point approximation is valid.

It seems that the degeneracy of the K-points results in identical contribution of each Dirac point in all of the physical quantities when the Fermi energy is close to the Dirac points. However, it should be noted that, this is not the case for some of the quantities which directly depending on the direction of the transferred wave number. In this case due to the anisotropic position of the Dirac points in the Brillouin zone, each of the Dirac points has not identical contribution for this type of the quantities, even when the Dirac point approximation is valid. Meanwhile, since the inter-valley transitions could take place between the different Dirac cones, these type of transitions cannot be captured within the single Dirac cone approximation.

Anisotropic Friedel oscillations in two-Dimensional structures have been observed before.⁵¹ However, in the present case the anisotropic effects are direct manifestation of non-identical contribution of Fermi circles and Dirac points in wave number dependent quantities. Some of the physical quantities, such as dielectric function, are given by integration over the Brillouin zone as expressed in Eq. (3). This integration goes beyond the states in which the Dirac point approximation and the linear dispersion relation no longer valid. However distribution function at low temperatures and Fermi energies picks up the contribution of the states which were located near to the Dirac points. Nevertheless for evaluating non-scalar quantities that depending on the wave number and its direction we should consider that the orientation of the wave number, q , (relative to the position vector of the Dirac points in k-space) determines the contribution of each Dirac point. It can be clearly demonstrated that the dielectric function shows anisotropic directional dependence in q -space.

It should be noted that increasing of the Fermi energy results in deformation of circle-like Fermi curves (Fermi-circles) of low Fermi energies around the Dirac points.⁷ In this case the isotropic form of the Fermi circles change into the trigonal-shaped contours (known as trigonal warping effect) and the isotropic form of the Fermi curve around of the Dirac points has totally been removed at high Fermi energies. This type of deformation could results in a new source of anisotropy at high Fermi energies which could be captured within the single cone approximation. Meanwhile trigonal warping induced anisotropy has not been considered in the current work which was limited to the low Fermi energies.

At low Fermi energies optical transitions around each Dirac points, where take place within a single Fermi circle, have the main contribution in the dielectric function of the honeycomb systems. This manifests itself as a central peak of the dielectric function in the middle of the Brillouin zone. It could be shown that beyond the Dirac point approximation the central peak contains the contribution of all of the Dirac points via the inter-band transitions.

When the Fermi energy is close to Dirac points ($E_F = 0$) and at the high wave length limit ($q \ll |K_D - K'_D|$) the occupation factor $f_k^s - f_{k'}^{s'}$ could have a significant value only when the k and k' states are close to a single Dirac point of different bands ($s \neq s'$). Meanwhile the Kronecker delta, $\delta_{\vec{k}, \vec{k} + \vec{q}}$, in the expression of the polarization indicates that the contribution of the Dirac points should be selected by Γ -point ($\vec{q} = 0$). Since at this limit the main contribution is due to the intra-valley transitions which take place near the Dirac points in which $k \approx K_D$ and $k' \approx K_D$ therefore the mentioned Kronecker delta, which reflects the momentum conservation, imposes that the contribution of the Dirac points should be manifest themselves at the Γ -point ($\vec{q} \approx 0$) of the q -space.

The mentioned argument reveals the fact that the central peak (Figs. 5 and 6) of the dielectric function is exactly sum of all of the intra-valley contributions from each Dirac point. In this case since the main contribution belongs to the case of zero transferred momentum ($q \sim 0$) the question of the anisotropy in q -space seems to be irrelevant at $E_F = 0$. Although the contribution of the intra-valley transitions are dominant at $q \sim 0$, however, this is not the case for the wave numbers within the

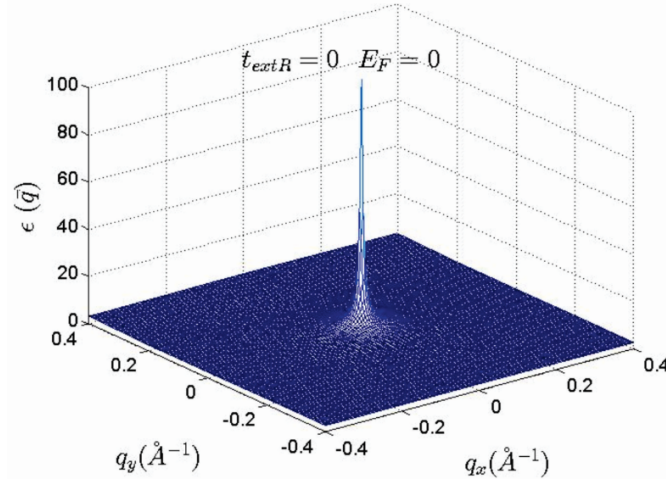


Figure 5. k -space dielectric function of monolayer graphene at $t_{extR} = 0$. Additionally it was assumed that the intrinsic spin-orbit coupling has been also negligible. This enables us to compute the net band induced anisotropic effects.

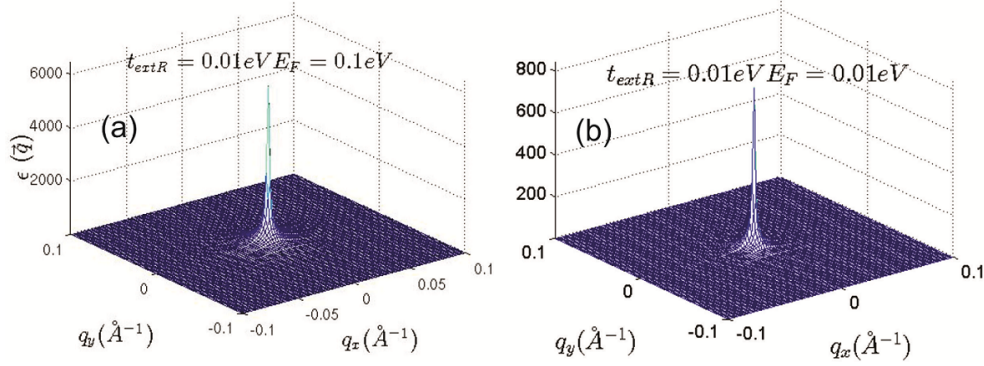


Figure 6. k -space dielectric function of monolayer silicene and germanene $t_{extR} = 0.01 eV$.

range of $|K_D - K'_D| - 2k_F \leq q < |K_D - K'_D| + 2k_F$. It should be noted that the contribution of inter-valley transitions between different Dirac points ($q \sim |K_D - K'_D|$) are not identical. In this case the contribution of each pair of contributing Dirac point (\mathbf{K}_D and \mathbf{K}'_D) has been determined by the direction of the \vec{q} vector.

In order to obtain the anisotropic effects which have been induced merely by band energy we have to switch off both types of the spin orbit couplings. It was reported that the Rashba coupling strength in graphene is greater than the intrinsic spin orbit interaction.⁵² Therefore one can ignore intrinsic spin orbit coupling in monolayer graphene. At zero Rashba interaction both intrinsic and extrinsic spin-orbit couplings are absent. This enables us to obtain the anisotropic effects which could be induced merely by band energy. Dielectric function at zero Rashba coupling and zero Fermi energy ($E_F = 0$) has been obtained as depicted in Fig. (5). At the first look it seems that there is no anisotropy in the dielectric function of the honeycomb structures (Figs. 5 and 6), however, it should be noted that the anisotropy of the dielectric function has been hidden behind the large central peak at $q \sim 0$. The amount of the dielectric anisotropy is very small in comparison with the value of the dielectric function at the Γ -point. Accordingly this fact prevents the identification of the directional dependence of the dielectric function. At low wave numbers i.e. in the range of the intra-valley transitions dielectric function seems to be quite isotropic in q -space Fig. (7 (a) and (b)). However, far from the central region if we select different symmetric slices of the dielectric surface, the anisotropy of the dielectric function will be evident Fig. (7 (c) and (d)). A similar discussion holds for the case of silicene and germanene where as shown in Figs. 8 and 9 dielectric function has completely different behavior on symmetrically chosen slices, especially far enough the Γ point. These figures evidently show that for different directions in the k -space behavior of the dielectric function are quite different. This reveals that the contributing inter-valley transitions in finite wave length limit ($q \sim |K_D - K'_D|$) introduce the anisotropic behaviors.

As discussed before band induced anisotropic effects (see Fig. 3) have been reflected in the Friedel oscillations of the graphene-like structures illustrated in Figs. 10 and 11. The anisotropy of the dielectric function as discussed before is due

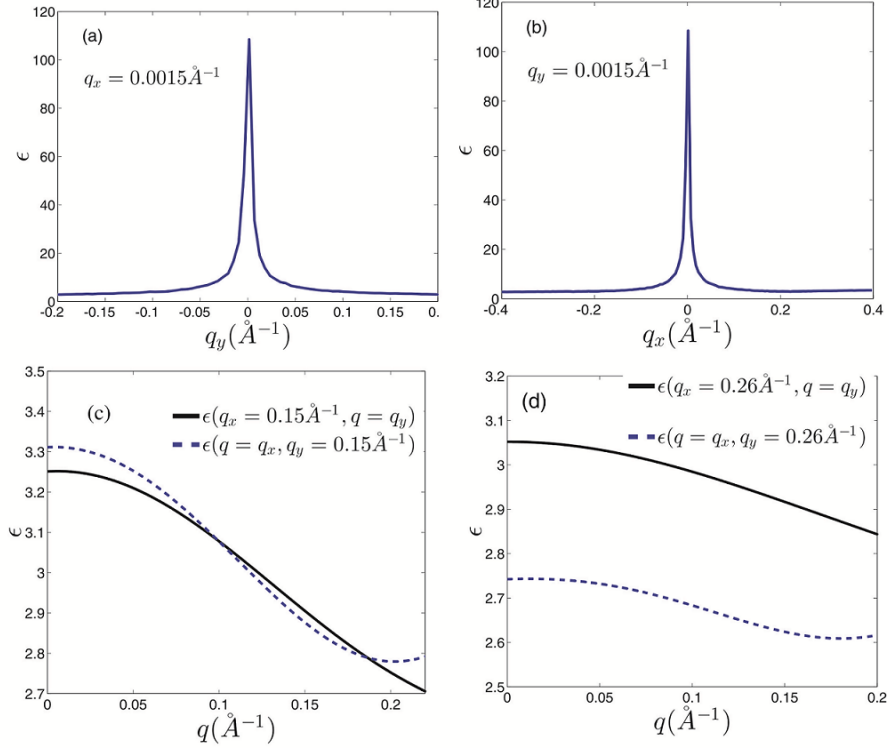


Figure 7. Dielectric function of monolayer graphene at different symmetrically chosen slices for $t_{extR} = 0$ in k -space. (a) At $q_x = 0.0015\text{\AA}^{-1}$ plane. (b) $q_y = 0.0015\text{\AA}^{-1}$ plane. (c) At $q_x = 0.15\text{\AA}^{-1}$ and $q_y = 0.15\text{\AA}^{-1}$ slices. (d) At $q_x = 0.26\text{\AA}^{-1}$ and $q_y = 0.26\text{\AA}^{-1}$ planes. Anisotropic effects appear far away from the origin where the contribution of the inter-valley transitions should be taken into account.

to the non-identical contribution of the Dirac points and the nonlinear part of the spectrum cannot contribute in dielectric function when the Fermi level is close to the Dirac points. Increasing the Rashba coupling strength slightly modifies the Friedel oscillations in silicene, however the change in monolayer graphene is relatively more pronounced compared to that of other selected honeycomb structures where Figs. (10 and 11) exactly indicates this fact. This could be explained if we consider relatively large and dominant intrinsic spin-orbit coupling in silicene.

As shown in the figure (10) the anisotropic Friedel oscillations have been observed even when the Rashba coupling strength is very low or zero. It can be inferred from the results of the current work that the Rashba coupling is less effective in the generation of the anisotropy. Therefore one can conclude that the anisotropy of the dielectric function and Friedel oscillations mainly depends on the anisotropy of the band structure in k -space.

There are several studies which have been performed in this field, aiming at an accurate quantitative prediction of dynamical dielectric function, screened charged impurity potential and Friedel oscillations in graphene-like materials. It was realized that the long-distance decay of Friedel oscillations in graphene depends on the symmetry of the scatterer.⁵³ In addition a faster, $\delta n \sim 1/r^3$, decay in comparison with conventional 2D electron systems has been observed in Friedel oscillations of a localized impurity inside the monolayer graphene within the Dirac point approximation.^{29,53} However, $1/r$ decay has been reported for bilayer graphene⁵⁴ and strong asymmetry and an inverse square-root decay has also been obtained for an anisotropic graphene-like structure when one of the nearest-neighbor hopping amplitudes is different from the others.⁵⁵ Recently in rhombohedral graphene multi-layers, $1/r$ decay has been observed for impurity induced Friedel oscillations.⁵⁶ Completely isotropic behavior has been reported for the potential of a screened charged impurity, Friedel oscillations²⁸⁻³¹ and static dielectric function⁴³ within the Dirac point approximation in graphene. Similarly the Dirac point approximation results in isotropic screened potential of a charged impurity in other graphene-like materials such as silicene and germanene.²³

The studies based on Dirac point approximation give the correct physics of the high wave length limit ($q \ll k_F$) at $E_F = 0$ where inter-valley transitions could not contribute in the physical processes. In the absence of the spin-orbit couplings by using the massless linear Dirac spectrum it was also shown that short wavelength spatial dependence of the local density of states

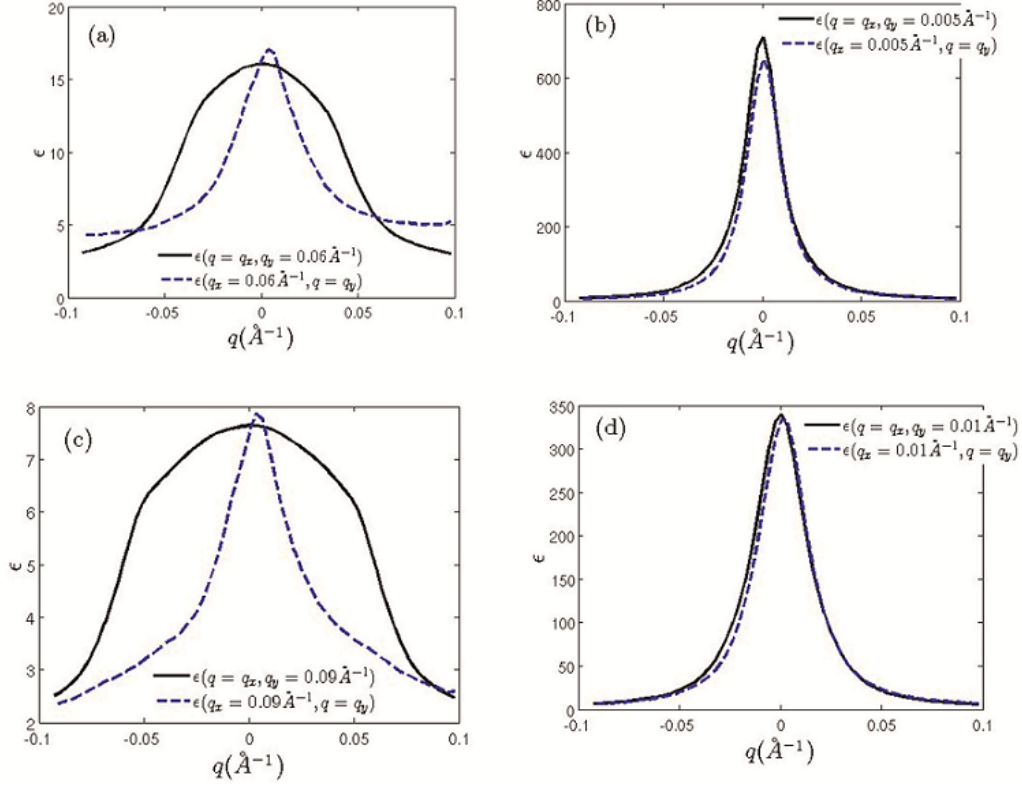


Figure 8. Dielectric function of monolayer silicene at different symmetrically chosen slices for $t_{extR} = 0.01\text{eV}$ in k -space. (a) At $q_\alpha = 0.06\text{\AA}^{-1}$ planes ($\alpha = x, y$). (b) $q_\alpha = 0.005\text{\AA}^{-1}$ planes. (c) At $q_\alpha = 0.09\text{\AA}^{-1}$ slices. (d) At $q_\alpha = 0.01\text{\AA}^{-1}$ planes. Anisotropic effects appear far away from the origin where the contribution of the inter-valley transitions is dominant.

leads to anisotropic Friedel oscillations which has the form⁵⁷

$$\delta n(r) \sim c(\vec{r})\rho_0(E_F)\frac{\sin(2k_F r)}{r^2}. \quad (9)$$

In which $c(\vec{r})$ is the short wavelength spatial dependence factor and $\rho_0(E)$ is the density of states. Anisotropic dependence of the Friedel oscillations has been introduced by $c(\vec{r})$ factor which was found to be invariant under threefold rotations.⁵⁷ However, if the impurity could not produce inter-valley scatterings this factor is reduced to a constant number.⁵⁷ Therefore the anisotropic effects have been removed in the absence of inter-valley transitions.⁵⁷ In the current study we have observed that for finite Fermi energies $0 < E_F \leq 1\text{eV}$ even intra-valley transitions are the source of the anisotropic behaviors at linear energy dispersion regime.

In the case of the single valley band structures where all of the transitions should be considered as intra-valley transitions. The wave length of the Friedel oscillations is modulated by Fermi wave number. However it can be easily shown that this is not the case for multi-valley band structures. In which the inter-valley transitions could contribute in the dielectric function. As indicated in Eq. (9) it was expected that the wavelength of the Friedel oscillations should be modulated by the Fermi wave-vector k_F .⁵⁷ Where the long range behavior of the local density of states has been obtained within the single valley approximation and linear dispersion relation.⁵⁷ The possible transferred momentums, q , determine the oscillation wavelength of the induced charged and for single valley band structures in two-dimensional systems typical transferred momentum is $q \sim 2k_F$. However it should be noted that for a typical graphene Fermi energy e.g. $E_F = 0.1\text{eV}$ one can obtain $k_F = E_F/(\hbar v_F) = 0.0152\text{\AA}^{-1}$. Therefore the oscillation wavelength that corresponds to the intra-valley transitions is about $\lambda_{intra} = 2\pi/2k_F \sim 200\text{\AA}$. On the other hand in the present case the inter-valley transitions with momentum transfer of $q \sim |\mathbf{K} - \mathbf{K}'| \pm 2k_F$ correspond to the oscillations with wavelength of $\lambda_{inter} = 2\pi/(|\mathbf{K} - \mathbf{K}'| \pm 2k_F)$. The wavelengths of the oscillations in the current work for monolayer graphene are in the following range $7\text{\AA} \lesssim \lambda_{inter} \lesssim 13\text{\AA}$ that are at the same order of the inter-valley transition wavelengths given by $\lambda_{inter} = 2\pi/(|\mathbf{K} - \mathbf{K}'| \pm 2k_F)$. For example the distance between two successive Dirac points in graphene is about $\Delta K = |K - K'| \sim 1.7\text{\AA}^{-1}$. Therefore the average momentum transfer between these Dirac points is $q \sim |K - K'|/2 = 0.85\text{\AA}^{-1}$ then $\lambda_{inter} = 2\pi/\Delta K = 7.37\text{\AA}$.

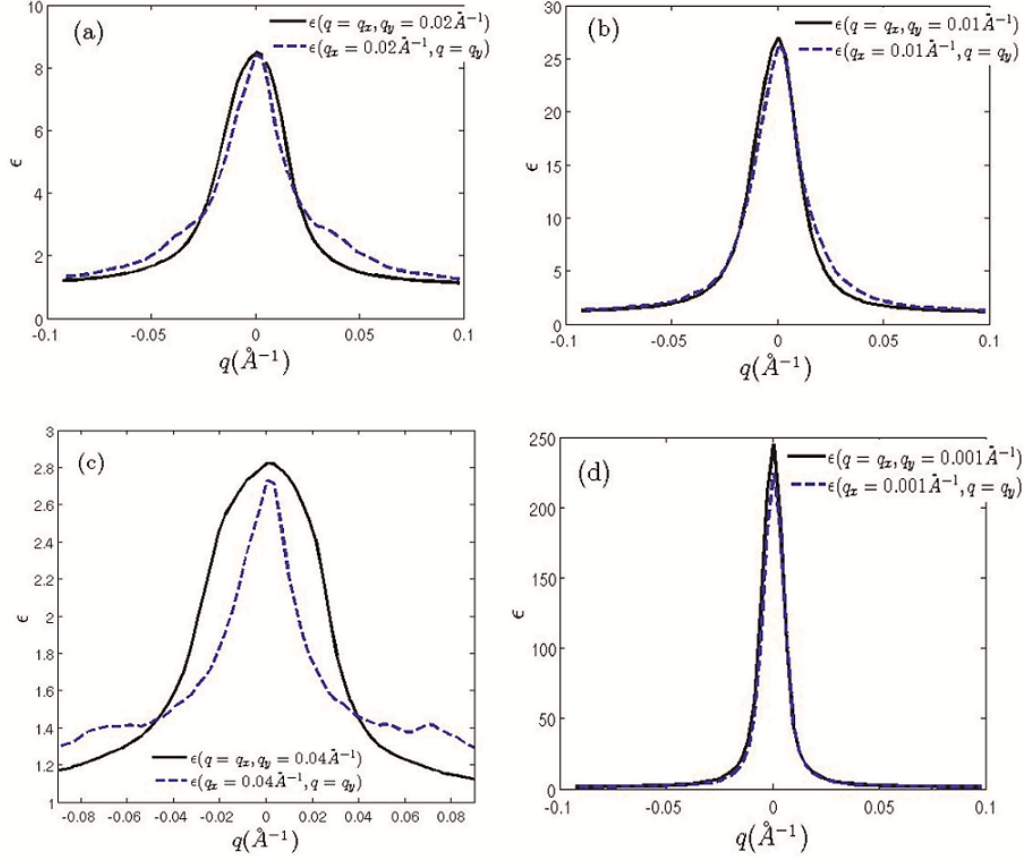


Figure 9. Dielectric function of monolayer silicene at different symmetrically chosen slices for $t_{extR} = 0.01\text{eV}$ in k -space. (a) At $q_\alpha = 0.02\text{\AA}^{-1}$ planes ($\alpha = x, y$). (b) $q_\alpha = 0.01\text{\AA}^{-1}$ planes. (c) At $q_\alpha = 0.04\text{\AA}^{-1}$ slices. (d) At $q_\alpha = 0.001\text{\AA}^{-1}$ planes. Anisotropic effects appear far away from the origin where the contribution of the inter-valley transitions is dominant.

The numerical results indicate that the wavelength of the oscillations is less-sensitive to the value of the Fermi energy. This can be realized if we consider that $|\mathbf{K} - \mathbf{K}'| \gg 2k_F$ for intermediate Fermi energies.

Decay rate of the Friedel oscillations are determined by fitting to the numerical results. We have examined several decay rates such as $1/r$, $1/r^2$ and $1/r^3$. Numerical fitting shows that the $1/r$ decay rate is much more close to the computational data profile. More precisely decay rate is actually $1/r^{1+\eta}$ where $0 < \eta < 0.2$.

Another important issue about the Friedel oscillations is that how sharp the mentioned density anisotropy really is? In this way we have obtained the angular dependence of the induced density at different distances as depicted in Fig. (12). As indicated in this figure the anisotropy of the Friedel oscillations increases by distance. It can be realized that the angular dependence of the induced density is so sharp at intermediate distances. This provides more detectable condition for observation of the anisotropy.

Interestingly it was shown that the Friedel oscillations in graphene have a strong sublattice asymmetry.⁵⁸ These calculations have been performed beyond the Dirac point approximation within the Born approximation which can be employed for weak scattering potentials and the stationary phase approximation (SPA) has also been applied for Brillouin zone integrations.⁵⁸ Anisotropic Friedel oscillations could also be inferred from the numerical results of the recent work in the absence of the spin-orbit interactions especially over short distances.

Finally it is important to note, the anisotropy of the dielectric function suggests that the orientation of the bases vectors of the honeycomb lattice could be determined by full optical measurements. Since dynamical dielectric function of the graphene-like materials are possibly have the same anisotropic nature. Therefore the absorption spectra of the system should be anisotropic. Accordingly, the real space orientation of the basis vectors could be explored since the absorption spectra leads to identification of the band energy configuration in k -space.

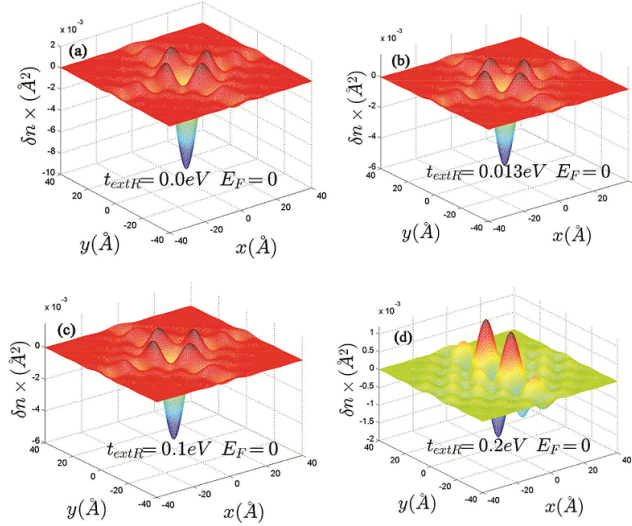


Figure 10. Real space anisotropic Friedel oscillations in monolayer graphene at different Rashba couplings. (a)-(c) As shown in these figures the Rashba interaction has not a significant influence on the Friedel oscillations at intermediate Rashba coupling strength. (d) Unlike to the previous case for $t_{extR} = 0.2 \text{ eV}$ Friedel oscillations are not similar even for x and y directions.

References

1. Novoselov, K. S. *et al.* Electric field effect in atomically thin carbon films. *Science* **306**, 666–669 (2004).
2. Geim, A. K. & Novoselov, K. S. The rise of graphene. *Nature Materials* **6**, 183–191 (2007).
3. Dávila, M. E. & Le Lay, G. Few layer epitaxial germanene: a novel two-dimensional dirac material. *Scientific reports* **6** (2016).
4. Xu, Y. *et al.* Large-gap quantum spin hall insulators in tin films. *Phys. Rev. Lett.* **111**, 136804 (2013).
5. Zhu, F.-f. *et al.* Epitaxial growth of two-dimensional stanene. *Nature materials* **14**, 1020–1025 (2015).
6. Guzmán-Verri, G. G. & Voon, L. L. Y. Electronic structure of silicon-based nanostructures. *Phys. Rev. B* **76**, 075131 (2007).
7. Cahangirov, S., Topsakal, M., Aktürk, E., Şahin, H. & Ciraci, S. Two-and one-dimensional honeycomb structures of silicon and germanium. *Phys. Rev. Lett.* **102**, 236804 (2009).
8. Liu, C.-C., Feng, W. & Yao, Y. Quantum spin hall effect in silicene and two-dimensional germanium. *Phys. Rev. Lett.* **107**, 076802 (2011).
9. Liu, F., Liu, C.-C., Wu, K., Yang, F. & Yao, Y. $d + i d'$ chiral superconductivity in bilayer silicene. *Phys. Rev. Lett.* **111**, 066804 (2013).
10. Chen, L. *et al.* Evidence for dirac fermions in a honeycomb lattice based on silicon. *Phys. Rev. Lett.* **109**, 056804 (2012).
11. Vogt, P. *et al.* Silicene: compelling experimental evidence for graphenelike two-dimensional silicon. *Phys. Rev. Lett.* **108**, 155501 (2012).
12. Chen, L. *et al.* Spontaneous symmetry breaking and dynamic phase transition in monolayer silicene. *Phys. Rev. Lett.* **110**, 085504 (2013).
13. Feng, B. *et al.* Evidence of silicene in honeycomb structures of silicon on ag (111). *Nano Letters* **12**, 3507–3511 (2012).
14. Lin, X. & Ni, J. Much stronger binding of metal adatoms to silicene than to graphene: A first-principles study. *Phys. Rev. B* **86**, 075440 (2012).
15. Takeda, K. & Shiraishi, K. Theoretical possibility of stage corrugation in si and ge analogs of graphite. *Phys. Rev. B* **50**, 14916 (1994).
16. Durgun, E., Tongay, S. & Ciraci, S. Silicon and iii-v compound nanotubes: Structural and electronic properties. *Phys. Rev. B* **72**, 075420 (2005).

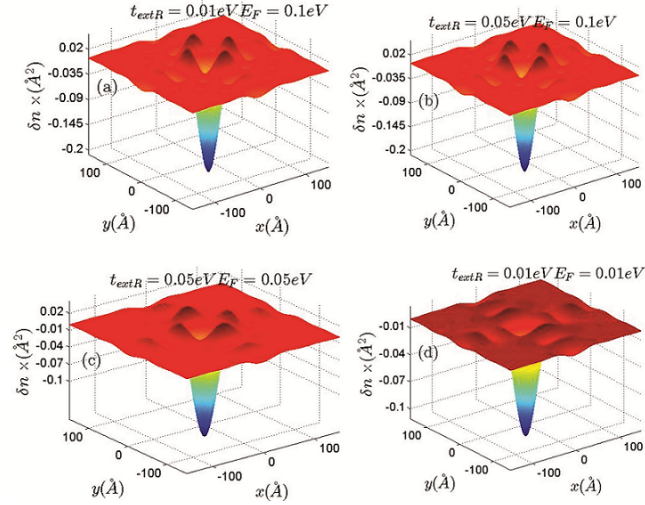


Figure 11. Real space anisotropic Friedel oscillations in monolayer silicene ((a) and (b)) and germanene ((c) and (d)) at different Rashba couplings. The Rashba interaction has not a significant influence on the Friedel oscillations.

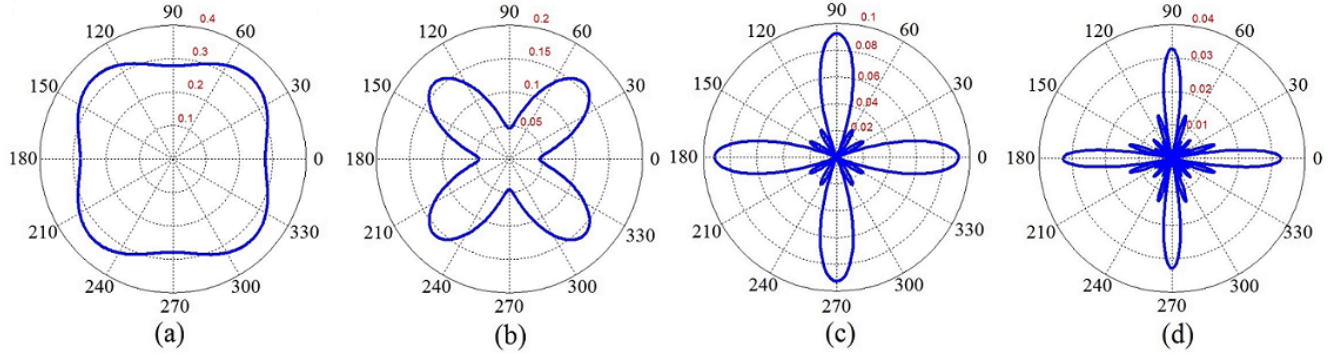


Figure 12. Angular dependence of the normalized graphene Friedel oscillations, $\delta n(r, \theta)/n_0$, for $t_{extR} = 0$, $E_F = 0.1t$ and $K_B T = 0$ at (a) $r = 4\text{\AA}$, (b) $r = 5\text{\AA}$, (c) $r = 14\text{\AA}$ and (d) $r = 25\text{\AA}$ in which we have defined $n_0 = \delta n(\mathbf{r} = 0)$.

17. Ezawa, M., Tanaka, Y. & Nagaosa, N. Topological phase transition without gap closing. *Scientific Reports* **3**, 2790 (2013).
18. Tahir, M. & Schwingenschlögl, U. Valley polarized quantum hall effect and topological insulator phase transitions in silicene. *Scientific Reports* **3**, 1075 (2013).
19. Padilha, J., Pontes, R., Schmidt, T., Miwa, R. & Fazzio, A. A new class of large band gap quantum spin hall insulators: 2d fluorinated group-iv binary compounds. *Scientific reports* **6**, 26123.
20. Mahan, G. D. *Many-particle physics* (Springer, 2000).
21. Grigorenko, A., Polini, M. & Novoselov, K. Graphene plasmonics. *Nature Photonics* **6**, 749–758 (2012).
22. Bonaccorso, F., Sun, Z., Hasan, T. & Ferrari, A. Graphene photonics and optoelectronics. *Nature Photonics* **4**, 611–622 (2010).
23. Tabert, C. J. & Nicol, E. J. Dynamical polarization function, plasmons, and screening in silicene and other buckled honeycomb lattices. *Phys. Rev. B* **89**, 195410 (2014).
24. Roldán, R. & Brey, L. Dielectric screening and plasmons in aa-stacked bilayer graphene. *Phys. Rev. B* **88**, 115420 (2013).
25. Liu, C.-C., Jiang, H. & Yao, Y. Low-energy effective hamiltonian involving spin-orbit coupling in silicene and two-dimensional germanium and tin. *Phys. Rev. B* **84**, 195430 (2011).
26. Ezawa, M. A topological insulator and helical zero mode in silicene under an inhomogeneous electric field. *New Journal of Physics* **14**, 033003 (2012).

27. Min, H. *et al.* Intrinsic and rashba spin-orbit interactions in graphene sheets. *Phys. Rev. B* **74**, 165310 (2006).
28. Scholz, A., Stauber, T. & Schliemann, J. Dielectric function, screening, and plasmons of graphene in the presence of spin-orbit interactions. *Phys. Rev. B* **86**, 195424 (2012).
29. Wunsch, B., Stauber, T., Sols, F. & Guinea, F. Dynamical polarization of graphene at finite doping. *New Journal of Physics* **8**, 318 (2006).
30. Gómez-Santos, G. & Stauber, T. Measurable lattice effects on the charge and magnetic response in graphene. *Phys. Rev. Lett.* **106**, 045504 (2011).
31. Cheianov, V. V. & Fal'ko, V. I. Friedel oscillations, impurity scattering, and temperature dependence of resistivity in graphene. *Phys. Rev. Lett.* **97**, 226801 (2006).
32. Chang, H.-R., Zhou, J., Zhang, H. & Yao, Y. Probing the topological phase transition via density oscillations in silicene and germanene. *Phys. Rev. B* **89**, 201411 (2014).
33. Schmidt, M. J., Golor, M., Lang, T. C. & Wessel, S. Effective models for strong correlations and edge magnetism in graphene. *Phys. Rev. B* **87**, 245431 (2013).
34. Quhe, R. *et al.* Does the dirac cone exist in silicene on metal substrates? *Scientific Reports* **4**, 5476 (2014).
35. Ezawa, M. Spin valleytronics in silicene: Quantum spin hall–quantum anomalous hall insulators and single-valley semimetals. *Phys. Rev. B* **87**, 155415 (2013).
36. Bychkov, Y. A. & Rashba, E. I. Oscillatory effects and the magnetic susceptibility of carriers in inversion layers. *Journal of physics C: Solid state physics* **17**, 6039 (1984).
37. Ando, T., Fowler, A. B. & Stern, F. Electronic properties of two-dimensional systems. *Rev. Mod. Phys.* **54**, 437 (1982).
38. Giuliani, G. & Vignale, G. *Quantum theory of the electron liquid* (Cambridge university press, 2005).
39. Kaasbjerg, K., Thygesen, K. S. & Jauho, A.-P. Acoustic phonon limited mobility in two-dimensional semiconductors: Deformation potential and piezoelectric scattering in monolayer mos 2 from first principles. *Phys. Rev. B* **87**, 235312 (2013).
40. Pyatkovskiy, P. Polarization function and plasmons in graphene with a finite gap in the quasiparticle spectrum. *J. Phys.: Conf. Ser.* **129**, 012006 (2008).
41. Pyatkovskiy, P. Dynamical polarization, screening, and plasmons in gapped graphene. *Journal of Physics: Condensed Matter* **21**, 025506 (2009).
42. Gorbar, E., Gusynin, V., Miransky, V. & Shovkovy, I. Magnetic field driven metal-insulator phase transition in planar systems. *Phys. Rev. B* **66**, 045108 (2002).
43. Hwang, E. & Sarma, S. D. Dielectric function, screening, and plasmons in two-dimensional graphene. *Phys. Rev. B* **75**, 205418 (2007).
44. Sensarma, R., Hwang, E. & Sarma, S. D. Dynamic screening and low-energy collective modes in bilayer graphene. *Phys. Rev. B* **82**, 195428 (2010).
45. Scholz, A., Stauber, T. & Schliemann, J. Plasmons and screening in a monolayer of mos 2. *Phys. Rev. B* **88**, 035135 (2013).
46. Hwang, C. *et al.* Fermi velocity engineering in graphene by substrate modification. *Scientific Reports* **2**, 590 (2012).
47. Hwang, E. & Sarma, S. D. Screening, kohn anomaly, friedel oscillation, and rkky interaction in bilayer graphene. *Phys. Rev. Lett* **101**, 156802 (2008).
48. Hubbard, J. The description of collective motions in terms of many-body perturbation theory. ii. the correlation energy of a free-electron gas. *Proceedings of the Royal Society of London. Series A. Mathematical and Physical Sciences* **243**, 336–352 (1958).
49. Singwi, K., Sjölander, A., Tosi, M. & Land, R. Electron correlations at metallic densities. iv. *Phys. Rev. B* **1**, 1044 (1970).
50. Deng, T. & Su, H. Orbital-dependent electron-hole interaction in graphene and associated multi-layer structures. *Scientific Reports* **5**, 17337 (2015).
51. Hofmann, P. *et al.* Anisotropic two-dimensional friedel oscillations. *Phys. Rev. Lett.* **79**, 265 (1997).
52. Dedkov, Y. S., Fonin, M., Rüdiger, U. & Laubschat, C. Rashba effect in the graphene/ni (111) system. *Phys. Rev. Lett* **100**, 107602 (2008).

53. Cheianov, V. V. Impurity scattering, friedel oscillations and rky interaction in graphene. *The European Physical Journal Special Topics* **148**, 55–61 (2007).
54. Bena, C. Effect of a single localized impurity on the local density of states in monolayer and bilayer graphene. *Phys. Rev. Lett.* **100**, 076601 (2008).
55. Dutreix, C., Bilteanu, L., Jagannathan, A. & Bena, C. Friedel oscillations at the dirac cone merging point in anisotropic graphene and graphenelike materials. *Phys. Rev. B* **87**, 245413 (2013).
56. Dutreix, C. & Katsnelson, M. I. Friedel oscillations at the surfaces of rhombohedral n -layer graphene. *Phys. Rev. B* **93**, 035413 (2016).
57. Bácsi, A. & Virosztek, A. Local density of states and friedel oscillations in graphene. *Phys. Rev. B* **82**, 193405 (2010).
58. Lawlor, J. A., Power, S. R. & Ferreira, M. S. Friedel oscillations in graphene: Sublattice asymmetry in doping. *Phys. Rev. B* **88**, 205416 (2013).

Author contributions statement

All authors contributed to the numerical programming. A. Phirouznia and T. Farajollahpour carried out the discussion and analysed the results. In addition final version of the manuscript has been reviewed by A. Phirouznia and T. Farajollahpour.

Additional information

Competing financial interests: The authors declare no competing financial interests.